Stripmap Phase Gradient Autofocus

H. J. Callow, M. P. Hayes, and P. T. Gough
Acoustics Research Group,

Dept. of Electrical and Computer Engineering,
University of Canterbury,
Private Bag 4800, Christchurch, NZ
{h.callow,m.hayes,p.gough}@elec.canterbury.ac.nz

***Abstract*— Current sonar autofocus techniques for blur removal originate in the radar community but have not provided a complete solution for Synthetic Aperture Sonar (SAS) imagery. The wide-beam, wide-band nature of SAS imagery makes implementation of Synthetic Aperture Radar (SAR) autofocus techniques difficult.**

This paper describes a generalisation of the standard Phase Gradient Autofocus (PGA) algorithm used in spotlight SAR that allows operation with stripmap SAS geometries. PGA uses prominent points within the target scene to estimate image blurring and phase errors. We show how PGA can be generalised to work with wide-band, wide-beam stripmap geometries.

The SPGA method works by employing wavenumber domain 2D phase estimation techniques. The 2D phase errors are related to aperture position errors using the wavenumber transform. Robust sway estimates are obtained by using redundancy over a number of target points.

We also present an improved Phase Curvature Autofocus (PCA) algorithm using the wavenumber transform. Preliminary results from the two algorithms (both on field-collected and simulated data sets) are presented and related to those obtained using previous methods. A discussion of SPGA's benefits over traditional algorithms and the limitations of the SPGA algorithm. The SPGA algorithm was found to perform better than 2-D PCA on both simulated and field-collected data sets. Further testing on a variety of target scenes and imagery is required to investigate avenues of autofocus improvement.

I. Introduction

Synthetic Aperture Sonar (SAS) provides high-resolution seafloor imaging by coherently combining the echoes received over a number of transmitted pings. Synthetic apertures can be achieved that are much longer than physical apertures, especially at low frequencies. Synthetic apertures can also be tailored to achieve a constant along track resolution with range.

The disadvantage of synthesising long apertures is that it is difficult to constrain (or measure) the sonar path to the accuracy required for coherent processing. Given sufficient unknown sway, the reconstructed image is severely blurred. Typically the amount of sway during aperture creation sufficient to cause blurring is of the order of $\lambda/16$ for low-order sway and $\lambda/60$ for high-order sway [1][1]. Constraining the motion of a tow-body with the use of a fixed guide or rail has been popular in the past to prove the concept of synthetic aperture sonar but is limited for practical use. High-drag nose towed towfish have been employed to successfully reduce the sway and autonomous underwater vehicles (AUVs) have been proposed as more stable SAS platforms. Ideally, SAS systems would be able to produce blur-free imagery without requiring strict path constraints and thus be deployed off any craft of opportunity.

There are two common approaches to removing the blurring caused by the unknown sonar motion. The first is to instrument the sonar platform with an extremely accurate inertial navigation system (INS) to monitor the path followed by the sonar. These systems are expensive (but getting cheaper) and so the second approach is to estimate the sonar motion from the recorded echo data. The techniques that implement this are usually referred to as "autofocus" or "micro-navigation" techniques. Both data-driven micro-navigation and autofocus techniques attempt to solve essentially the same problem, that of estimating the path of the sonar from the data (and correcting the output images, possibly in iterative fashion).

Many autofocus techniques for synthetic aperture sonar and radar have been proposed in the literature. Essentially these either use strong point-like scatterers or the ensemble of weak scatterers that produce the seafloor reverberation.

The most popular technique for SAR autofocus is Phase Gradient Autofocus (PGA) [3], [4]. However, the application of this technique is restricted to spotlight imaging geometries rather than the stripmap modes common in SAS imaging. In spotlight operation, a tight sonar beam is steered onto the region of interest whereas the more general stripmap configuration images the scene with an unsteered wide sonar beam. PGA has been applied to the stripmap SAS by mosaicing the results from small sections of the aperture (mPGA) [5].

A more promising variation of PGA applicable to stripmap operation is PCA (Phase Curvature Autofocus) [6]. However, as shown in this paper, PCA cannot estimate local linear phase errors.

This paper presents an algorithm similar to PCA that allows phase gradients to be estimated rather than phase curvatures. This algorithm is applicable to stripmap operation hence we call this algorithm Stripmap Phase Gradient Autofocus (SPGA). We start by recapping the effect motion error has on synthetic aperture imagery, then present a modified PCA algorithm for sway estimation in the presence of 2-D blurring. This is followed by a description of SPGA and a comparison

[1]Although the constraint is on the rate-of-change of sway it is more commonly expressed in terms of absolute accumulated sway [2].

Report Documentation Page

Form Approved
OMB No. 0704-0188

1. REPORT DATE	2. REPORT TYPE	3. DATES COVERED
01 SEP 2003	**N/A**	**-**

4. TITLE AND SUBTITLE	5a. CONTRACT NUMBER
Stripmap Phase Gradient Autofocus	5b. GRANT NUMBER
	5c. PROGRAM ELEMENT NUMBER
6. AUTHOR(S)	5d. PROJECT NUMBER
	5e. TASK NUMBER
	5f. WORK UNIT NUMBER
7. PERFORMING ORGANIZATION NAME(S) AND ADDRESS(ES) **Acoustics Research Group, Dept. of Electrical and Computer Engineering, University of Canterbury, Private Bag 4800, Christchurch, NZ**	8. PERFORMING ORGANIZATION REPORT NUMBER
9. SPONSORING/MONITORING AGENCY NAME(S) AND ADDRESS(ES)	10. SPONSOR/MONITOR'S ACRONYM(S)
	11. SPONSOR/MONITOR'S REPORT NUMBER(S)

12. DISTRIBUTION/AVAILABILITY STATEMENT
Approved for public release, distribution unlimited

13. SUPPLEMENTARY NOTES
See also ADM002146. Oceans 2003 MTS/IEEE Conference, held in San Diego, California on September 22-26, 2003. U.S. Government or Federal Purpose Rights License., The original document contains color images.

14. ABSTRACT

15. SUBJECT TERMS

16. SECURITY CLASSIFICATION OF:			17. LIMITATION OF ABSTRACT	18. NUMBER OF PAGES	19a. NAME OF RESPONSIBLE PERSON
a. REPORT	b. ABSTRACT	c. THIS PAGE			
unclassified	**unclassified**	**unclassified**	**UU**	**8**	

of its performance relative to the modified PCA. These results are shown both for simulated and field-collected data. Finally, we discuss the limitations of SPGA and autofocus in general, draw our conclusions, and present recommendations for future research.

II. Motion effects

To understand the operation of SPGA it is necessary to consider the blurring caused by unknown motion errors. In general, the motion-affected pulse-compressed sonar data $\widetilde{ss}(t,u)$ can be related to the motion-free data $ss(t,u)$ using

$$\widetilde{ss}(t,u) = \mathcal{M}\left(ss(t,u); X(u)\right) \tag{1}$$

where $X(u)$ is the unknown position error as a function of the along-track position, u, t is the time delay related to range, and $\mathcal{M}$ is an operator describing the motion induced transformation. The goal of autofocus algorithms is to estimate $X(u)$ from $\widetilde{ss}(t,u)$ and to recover $ss(t,u)$.

The proposed autofocus algorithms operate on regions of the distorted reconstructed image $\widetilde{ff}(x,y)$,

$$\widetilde{ff}(x,y) = \mathcal{A}\left\{\widetilde{ss}(t,u)\right\}, \tag{2}$$

where $\mathcal{A}\{\}$ is an operator that represents the azimuth compression performed by the image reconstruction algorithm.

Using the notation of [7], the pulse-compressed signal may be described using a 2-D convolution of the target distribution ff with a range-variant point spread function H,

$$\widetilde{sS}(y,\omega) = |P(\omega)|^2 \int\!\!\int_{-\infty}^{\infty} ff(x_1,y_1) H(X(u)-x_1, u-y_1, \omega) dx_1 dy_1, \tag{3}$$

where the point spread function is the squared free space Green's function weighted by the beam pattern of the sonar

$$H(X(u)-x_1,u-y_1,\omega) = \frac{\exp\left(-jk\sqrt{(X(u)-x_1)^2+(u-y_1)^2}\right)}{(4\pi)^2\left((X(u)-x_1)^2+(u-y_1)^2\right)} \times B^2\left(\frac{\omega(u-y_1)D_y}{\sqrt{(X(u)-x_1)^2+(u-y_1)^2}}\right), \tag{4}$$

where $k=\omega/c$. To keep the mathematics manageable we have assumed 3-D scattering from point targets in the z plane of the sonar and thus have ignored elevation beam pattern effects. There are many other assumptions implicit in Eq. (4), primarily that the sonar does not move during the interval echoes are collected so that there is no temporal Doppler shift—the so-called "stop-and-hop" assumption.

The point spread function Eq. (4) can be simplified by assuming that the sway is small compared to the across-track target position, i.e., $|X(u)| \ll x_1$, so

$$H(X(u)-x_1,u-y_1,\omega) \approx \exp\left(-j2kX(u)\frac{x_1}{\sqrt{x_1^2+(u-y_1)^2}}\right) H(x_1,u-y_1,\omega). \tag{5}$$

Then using the substitution

$$\cos\theta(u) = \frac{x_1}{\sqrt{x_1^2+(u-y_1)^2}}, \tag{6}$$

where $\theta(u)$ is the angle from the sonar to a target at (x_1,y_1), Eq. (5) can be written as

$$H(X(u)-x_1,u-y_1,\omega) \approx \exp\left(-j2kX(u)\cos\theta(u)\right) H(x_1,u-y_1,\omega). \tag{7}$$

In narrowbeam applications $\cos\theta(u)\approx 1$, in which case

$$H(X(u)-x_1,u-y_1,\omega) \approx \exp\left(-j2kX(u)\right) H(x_1,u-y_1,\omega). \tag{8}$$

This is the simple timing error approximation. In the narrowband case this further simplifies to

$$H(X(u)-x_1,u-y_1,\omega) \approx \exp\left(-j2k_0X(u)\right) H(x_1,u-y_1,\omega) \tag{9}$$

where $k_0=\omega_0/c$ is the carrier wavenumber.

Using the simple timing error approximation with Eq. (3), the pulse-compressed echo measured with a motion $X(u)$ can be related to the motion free pulse-compressed echo,

$$\widetilde{sS}(u,\omega) \approx sS(u,\omega)\exp\left(-j2kX(u)\right). \tag{10}$$

Describing the effect of a motion error on the reconstructed image is not straightforward since it depends on the form of $X(u)$. In the simple case of a small constant sonar sway ($X(u)=X$), there is no obvious effect on the reconstructed image; it is simply displaced in range[2]. When there is a small constant linear sway ($X(u)=\sigma u$), the reconstructed image is skewed,

$$\widetilde{ff}(x,y) \approx ff(x-\sigma y, y+\sigma x), \tag{11}$$

which for very small linear sway gradients σ and large offsets x_0 can be approximated by an along-track shear in y. Finally, higher order motion errors cause blurring.

III. Modified PCA algorithm

The standard PCA algorithm [6] developed for SAR neglects across-track image blurring and simply uses across-track image slices. SAS has large beamwidths and the across-track blurring is more significant. Here we present a modification of PCA that uses across-track blurring by considering regions around strong scattering targets. The key to the algorithm is how the motion estimates are combined since in a stripmap system the targets are only in view for a small portion of the sonar aperture.

In this algorithm we isolate patches of the reconstructed image around strong scatterers and relate phase errors back to the sonar motion using the wavenumber transform [8], [9]

$$k_y = \frac{u-y_m}{x_m}k_x, \tag{12}$$

[2]Some residual blurring is caused by focusing with the wrong focus parameters. This is akin to a slight Doppler-rate error or point-spread invariant quadratic blurring [2].

derived using the relation

$$\tan\theta = \frac{u - y_m}{x_m} = \frac{k_y}{k_x}. \tag{13}$$

Note that this relationship is valid only for the point at (x_m, y_m). The analysis may be extended for a small patch of data around that point if the sonar is in the far-field of the patch. The algorithm operates by taking the small patch about each strong scatterer in turn and calculating a sway estimate via the wavenumber transform; the transform is recalculated for each scatterer.

Starting with the pulse-compressed echo signal $ss(u,t)$, the modified PCA algorithm is:

Step 1: Fourier transform pulse-compressed echo data into the temporal frequency domain:

$$\widetilde{sS}(u,\omega) = \int_{-\infty}^{\infty} \widetilde{ss}(u,t)\exp(-j\omega t)\,dt. \tag{14}$$

Step 2: Correct for known sway $X(u)$, using Eq. (10).

Step 3: Reconstruct image $\widetilde{ff}(x,y)$ from $\widetilde{sS}(u,\omega)$, say using the wavenumber algorithm.

Step 4: Find prominent points in $\widetilde{ff}(x,y)$ and associate coordinates (x_m, y_m). Note that x_m and y_m do not need to be found to sub-pixel precision.

Step 5: Create masks $W_m(x,y)$ centred on (x_m, y_m), where

$$W_m(x,y) = \mathrm{rect}\left(\frac{x - x_m}{W_x}\right)\mathrm{rect}\left(\frac{y - y_m}{W_y}\right). \tag{15}$$

The sizes of these masks is a critical aspect of the algorithm. They need to be large enough to encompass the 2-D blurring of a point target but small enough to not include more than one strong target.

Step 6: Form images containing regions of interest by multiplying $\widetilde{ff}(x,y)$ by the masks $W_m(x,y)$,

$$\widetilde{ff}_m(x,y) = \widetilde{ff}(x,y)W_m(x,y). \tag{16}$$

Step 7: 2-D Fourier transform $\widetilde{ff}_m(x,y)$ to $\widetilde{FF}_m(k_x,k_y)$.

Step 8: Apply the wavenumber transform to form $\chi_m(k_x,u)$ from $\widetilde{FF}_m(k_x,k_y)$,

$$\chi_m(k_x,u) = \widetilde{FF}_m\left(k_x\frac{y_m - u}{x_m}, k_x\right). \tag{17}$$

Note that this requires an interpolation with sampled data.

Step 9: At this point we have M estimates of the phase error $\Phi_m(k_x,u)$ where

$$\Phi_m(k_x,u) = \text{phase}\left\{\chi_m(k_x,u)\right\}. \tag{18}$$

These phase errors are related to the residual sway at the i^{th} iteration by

$$\Phi_m(k_x,u) = k_x X_i(u), \tag{19}$$

which in the narrowbeam and narrowband case simplifies to

$$\Phi_m(k_x,u) \approx 2kX_i(u). \tag{20}$$

These phase error estimates cannot be directly averaged due to errors in the estimates of x_m and y_m. An error in x_m primarily generates a localised phase offset as well as a small hyperbolic along-track error.

An error in estimating y_m produces an along-track linear phase error. Moreover, y_m is the point of closest approach but not the true centre position of each target. Thus there is a local linear phase error and it is necessary to average the phase error curvatures since these are independent of y_m. The phase error curvatures are simply the second derivative of the along track phase errors. They can be computed using successive finite differences with a sheared product

$$\Delta^2\Phi_m(k_x,u) = \text{phase}\left\{\psi_m(k_x,y)\right\}, \tag{21}$$

where

$$\psi_m(k_x,u) = \chi_m(k_x,u+2\Delta u)\chi_m^{*2}(k_x,u+\Delta u)\chi_m(k_x,u). \tag{22}$$

Step 10: Average the phase error curvatures with an amplitude weighting using

$$\Delta^2\varphi(u) = \text{phase}\left\{\Psi(u)\right\} \tag{23}$$

where

$$\Psi(u) = \int_{-\infty}^{\infty}\sum_{m=1}^{M}\psi_m(k_x,u)dk_x. \tag{24}$$

Step 11: Double integrate the averaged phase error curvatures

$$\begin{aligned}\Delta\varphi(u) =& \Delta\varphi(y-\Delta u) + \Delta^2\varphi(y-\Delta u),\\ \varphi(u) =& \varphi(y-\Delta u) + \Delta\varphi(y-\Delta u).\end{aligned} \tag{25}$$

Step 12: Scale the phase error estimate by the wavelength of the centre frequency and estimate the residual sway

$$\hat{X}_i(u) = \frac{\varphi(u)}{2k_0}. \tag{26}$$

Step 13: Iterate algorithm until the residual sway is smaller than some threshold. The total estimated sway is the sum of the estimated residual sways from each iteration:

$$\hat{X}(u) = \sum_{i=1}^{I}\hat{X}_i(u). \tag{27}$$

While this algorithm has been described using continuous variables for convenience, in practice it is implemented using sampled variables. Furthermore, to reduce computation, offset variables are used such as the complex envelope.

IV. SPGA ALGORITHM

The disadvantage of PCA is that it does not estimate local linear sways; if there is not at least a point target per synthetic aperture length (i.e., if the aperture coverage is insufficient) then the reconstructed image can be disjoint.

SPGA overcomes this problem by estimating the local linear sway. SPGA's estimation is based on the observation that a local linear sway causes a displacement between the position of closest approach and the brightest point in the echo history [10]. Estimation of the local linear sway allows phase gradients rather than phase curvatures to be combined, improving autofocus performance in the presence of noise and preventing the image from becoming disjoint.

The effect of a linear sway in the spatial frequency (wavenumber) domain can be found from a 2-D Fourier transform of Eq. (11) to be similar to a frequency domain rotation

$$\widetilde{FF}(k_x, k_y) \approx FF(k_x - \sigma k_y, k_y + \sigma k_x). \tag{28}$$

Again, for small sway gradients σ, this approximately corresponds to a spatial frequency domain shift. Thus by estimating the spectral shift, σ may be estimated.

The SPGA algorithm operates as follows:

Step 1: Fourier transform pulse-compressed echo data into the temporal frequency domain.

$$\widetilde{sS}(u, \omega) = \int_{-\infty}^{\infty} \widetilde{ss}(u, t) \exp(-j\omega t)\, dt. \tag{29}$$

Step 2: Correct for known sway $X(u)$, using Eq. (10).

Step 3: Reconstruct image $\widetilde{ff}(x, y)$ from $\widetilde{sS}(u, \omega)$, say using the wavenumber algorithm.

Step 4: Find prominent points in $\widetilde{ff}(x, y)$ and associate coordinates (x_m, y_m). Note that x_m and y_m do not need to be found to sub-pixel precision.

Step 5: Create masks $W_m(x, y)$ centred on (x_m, y_m), where

$$W_m(x, y) = \text{rect}\left(\frac{x - x_m}{W_x}\right) \text{rect}\left(\frac{y - y_m}{W_y}\right). \tag{30}$$

Step 6: Form images containing regions of interest by multiplying $\widetilde{ff}(x, y)$ by the masks $W_m(x, y)$,

$$\widetilde{ff}_m(x, y) = \widetilde{ff}(x, y) W_m(x, y). \tag{31}$$

Step 7: 2-D Fourier transform $\widetilde{ff}_m(x, y)$ to $\widetilde{FF}_m(k_x, k_y)$.

Step 8: Determine the average along-track spatial energy density spectrum using

$$\beta_m(k_y) = \int_{-\infty}^{\infty} \left|\widetilde{FF}_m(k_x, k_y)\right|^2 dk_x. \tag{32}$$

Step 9: Calculate the centroid of the along-track spatial energy density spectrum allowing for circular wrapping using

$$\Delta k_{y_m} = \frac{k_{y\max}}{\pi} \text{phase}\left\{\iint \left|\widetilde{f}_m(k_x, k_y)\right|^2 dk_x \times \exp\left(j\frac{\pi k_y}{k_{y\max}}\right) dk_y\right\}. \tag{33}$$

Step 10: Estimate the local linear sway gradient,

$$\sigma_m = \frac{\Delta k_{y_m}}{2k_0}. \tag{34}$$

Step 11: Estimate the true target position (x'_m, y'_m)

$$x'_m = x_m, \tag{35}$$

$$y'_m = y_m - \sigma_m x_m. \tag{36}$$

Step 12: Phase correct the spatial spectrum to account for the estimated target position

$$\widetilde{FF}'_m(k_x, k_y) = \widetilde{FF}_m(k_x, k_y) \exp(-jk_x(x'_m - x_m)) \exp(-jk_y(y'_m - y_m)). \tag{37}$$

Step 13: Apply wavenumber transform to form $\chi_m(k_x, u)$ from $\widetilde{FF}'_m(k_x, k_y)$,

$$\chi_m(k_x, u) = \widetilde{FF}'_m\left(k_x \frac{y_m - u}{x_m}, k_x\right). \tag{38}$$

Step 14: Calculate the complex error gradient using a sheared product

$$\psi_m(k_x, u) = \chi_m(k_x, u + \Delta u)\chi^*_m(k_x, u). \tag{39}$$

Step 15: Average the phase error gradients with an amplitude weighting using

$$\Delta\varphi(u) = \text{phase}\{\Psi(u)\}, \tag{40}$$

where

$$\Psi(u) = \int_{-\infty}^{\infty} \sum_{m=1}^{M} \psi_m(k_x, u) dk_x. \tag{41}$$

Step 16: Integrate the averaged phase error gradients

$$\varphi(u) = \varphi(y - \Delta u) + \Delta\varphi(y - \Delta u). \tag{42}$$

Step 17: Scale the phase error estimate by the wavelength of the centre frequency and estimate the residual sway

$$\hat{X}_i(u) = \frac{\varphi(u)}{2k_0}. \tag{43}$$

Step 18: Iterate algorithm until the residual sway is smaller than some threshold. The total estimated sway is the sum of the estimated residual sways from each iteration:

$$\hat{X}(u) = \sum_{i=1}^{I} \hat{X}_i(u). \tag{44}$$

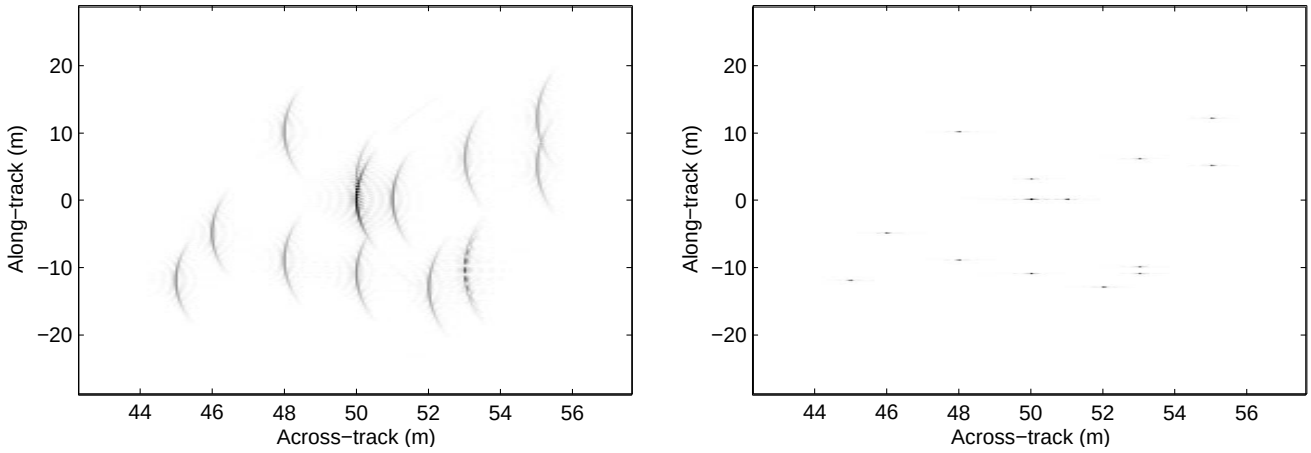

Fig. 1. Images containing a number of prominent points without sway: (a) magnitude of pulse-compressed echo history $ss(u,t)$, (b) magnitude of reconstructed image $ff(x,y)$.

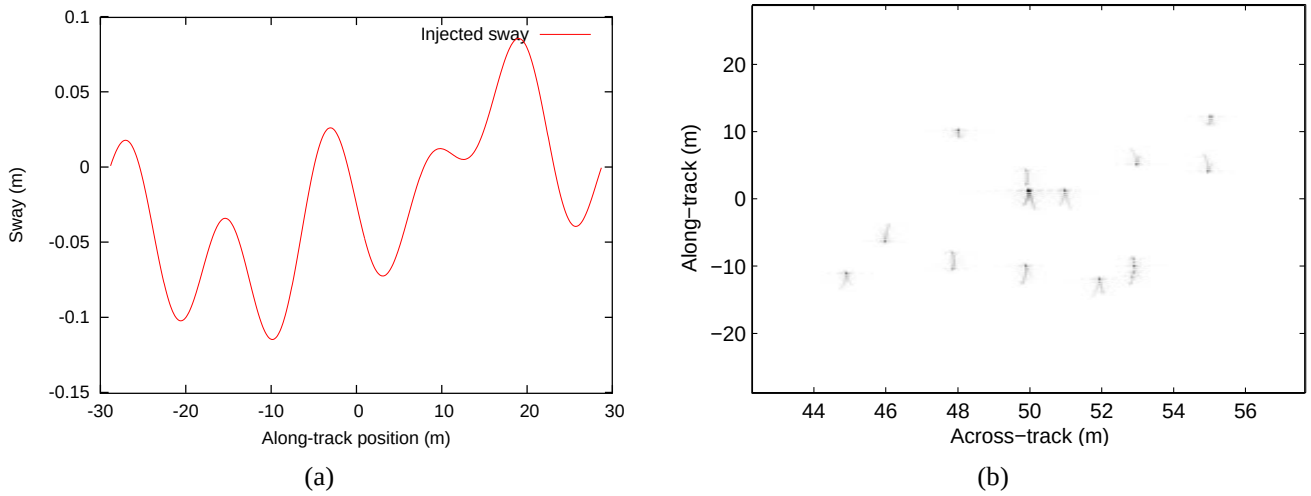

Fig. 2. Prominent points with distorting sway: (a) distorting sway $X(u)$, (b) magnitude of reconstructed image $\widetilde{ff}(x,y)$. Note the wide-band, 2-D blurring of the image.

V. Results

Fig. 1 shows pulse-compressed and corresponding reconstructed images used for simulation testing the algorithms. The system model chosen corresponds to the 30 kHz kiwiSAS-II sonar [11] with along-track sampling of $D/4$, transducer extent $D = 0.3$ m, and along-track resolution of 0.15 m.

Fig. 2 shows the effect of a mild sway on the scene. The sway is shown in Fig. 2(a) and has a peak-to-peak amplitude of 0.2 m (4 wavelengths). Fig. 2(b) shows the distorted reconstructed image–blurring and resolution degradation are evident. Along-track image resolution is position dependent and at worst is 3 m.

The sway estimated by the modified PCA and SPGA algorithms is shown along with the injected sway in Fig. 3(a). In this case, the result is from nine iterations of modified PCA/SPGA. The autofocus quality, like the original blurring itself, is space variant. In this case, the adjacent targets around (53,-10) and (50,1) cause small autofocus errors in an otherwise diffraction limited result. Fig. 3(b) allows another interpretation of image blurring by showing the estimated sway gradients. Sway gradient errors map directly to image blurring. Errors (and associated blurring) also occur at the edges of the scene where it lacks aperture coverage.

Using a simulated point-scatterer target scene in a noise-free situation, both modified PCA and SPGA shows clear image improvement and convergence (achieved within the first 3-4 iterations). SPGA gives better performance than PCA for the tested scene (there is no yaw in the simulation).

The SPGA algorithm was further tested with field-collected data. The data was collected was collected with the kiwiSAS-II in Sydney Harbour with the assistance of the Australian Defence Science and Technology Organisation (DSTO) in July of 2001. The scene consists of a number of target objects on a

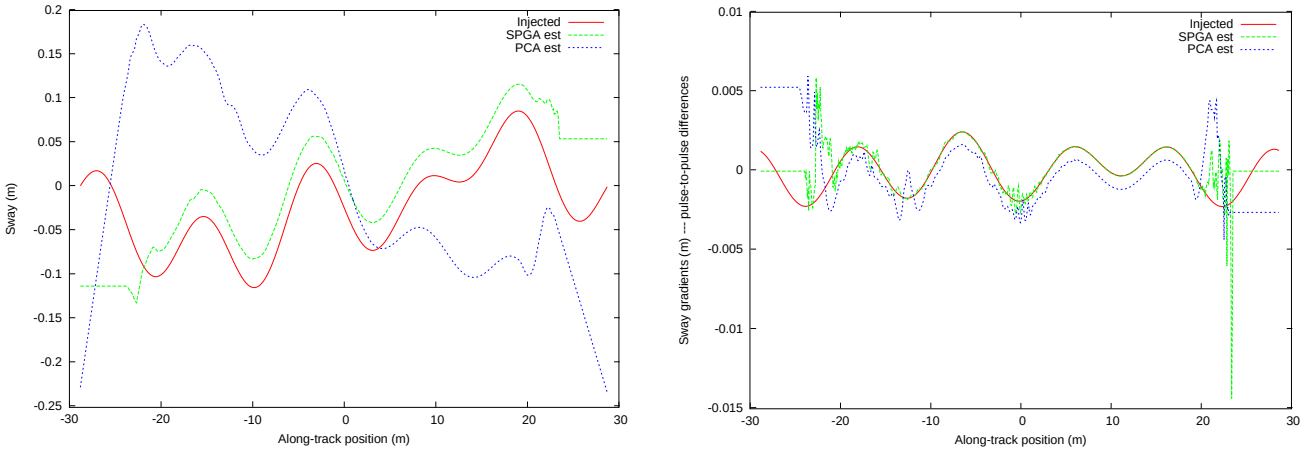

Fig. 3. Sway (a) and sway gradients (b) (metres) estimated by modified PCA and SPGA. The injected sway in both cases is denoted by the solid line.

sandy sea-floor and was collected with an along-track sample spacing of approximately $D/3$. The sonar was operating about 2 m from the sea-floor in approximately 10 m of water.

Fig. 4 shows the scene images before and after autofocus. The images are linear grey-scale and are clipped to -20 dB below the image peak. Salient features of the image include a 20 m long sonar calibration rail from (17,15) to (37,15) made up of triangular aluminium facets, an approximately 3 m long 0.5 m diameter pipe from (32,-11) to (32,-14) (reflections from both front and rear wall are visible) apparent shadowing at (12,-15). Other features are strong multi-path reflections from the pipe, a range-aliased target from (58,5) appearing at (6,5) and visible alias-lobes from mild aperture under-sampling. Note that the alias-lobe level is higher than expected for $D/3$ sampling because of spatial Doppler spectrum expansion caused by sway and a constant yaw offset.

Fig. 4(a) corresponds to the initial reconstructed image and Fig. 4(b) shows the SPGA autofocused image estimate. Note focus improvement and a reduction in side-lobe levels. The window size was reduced at each iteration to 0.8 of the size at the previous iteration from a starting size of 0.8 m by 5 m.

VI. Discussion

The main advantage of SPGA over PCA is that it can calculate phase gradients. Thus it can estimate the true positions of targets and does not suffer so badly when there are regions of poor target coverage. In addition, SPGA uses improved modelling over traditional techniques improving performance. However, there are a number of limitations caused by the requirement for a statistically homogeneous scence. These are:

Window size — SPGA windows individual targets to ensure that the phase signature of only one scatterer at a time is used. If a number of targets exist within the window, the path estimation gives poor results. Selecting many targets at different locations alleviates some of the symptoms.
A related problem exists if the window does not fully encompass target blurring. The algorithm is unable to estimate high-order blurring components leading to degraded path estimates (see [12]). SPGA, like PGA, starts with a wide window that decreases over time to allow estimation of the low-order path errors after the high-order errors.

Point scatterer assumption — In the derivation of SPGA the image scene was assumed to consist of a number of randomly placed point scatterers. The algorithm exploits the randomly varying scene phase structure to estimate the constant phase structure caused by the sonar sway. Any statistically homogeneous scene is suitable for SPGA operation, where the selected targets have zero average Fourier phase (the same as the Knox-Thompson and zero bispectral-phase priors used in astronomical imaging [13], [14]).
The selection of a strongly scattering target that has significant Fourier phase (often a strongly scattering extended target) leads to estimate biasing. The bias may be reduced by selecting point-like targets that have a high contrast [15]. Selecting many point-like targets is a useful way of ensuring the algorithm's input scene is statistically homogeneous.

Window separation — SPGA requires the input patches to be uncorrelated—to ensure statistical homogeneity. The selected patches should be well separated [15]. SPGA requires that the majority of energy comes from within the selected patch. Grating lobes (target energy from outside of the patch) caused by under-sampling of the aperture should be rejected.

Clutter information — The information contained in sea-floor clutter is useful for autofocus. SPGA currently ignores this source of information. However, we expect that SPGA is able to operate on clutter regions with a different patch selection policy. Clutter regions (on average) satisfy the requirement for a statistically homogeneous scene (even if the point-scatterer assumption does not hold) and

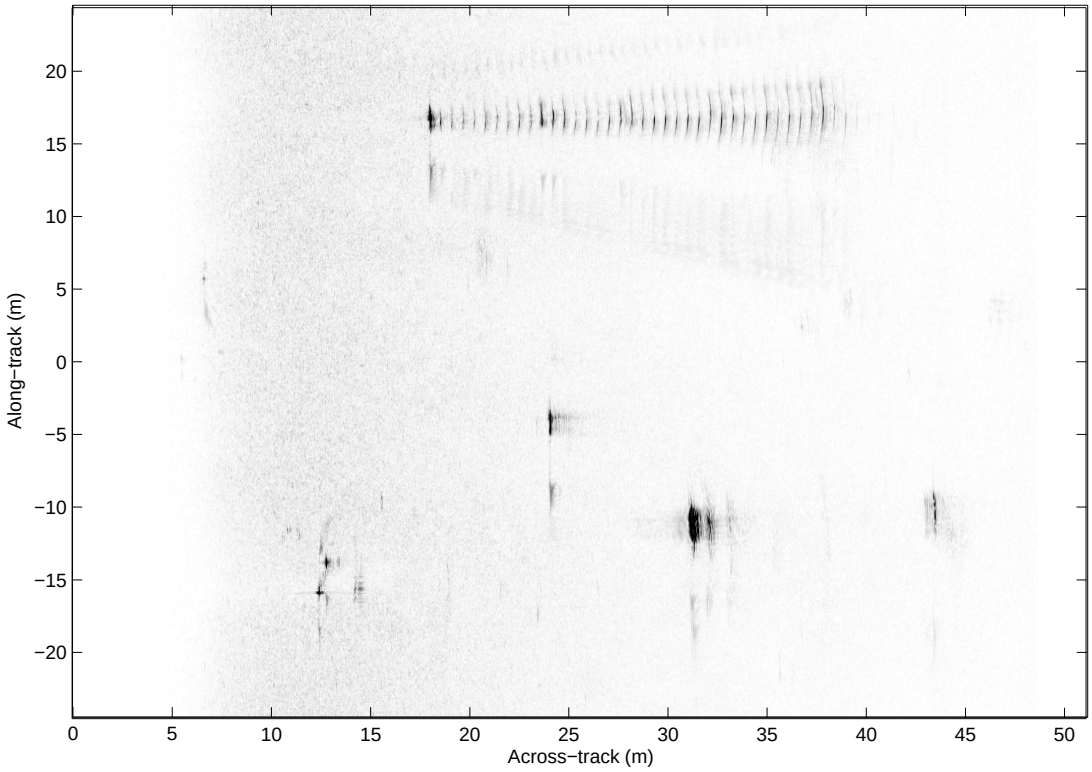

(a)

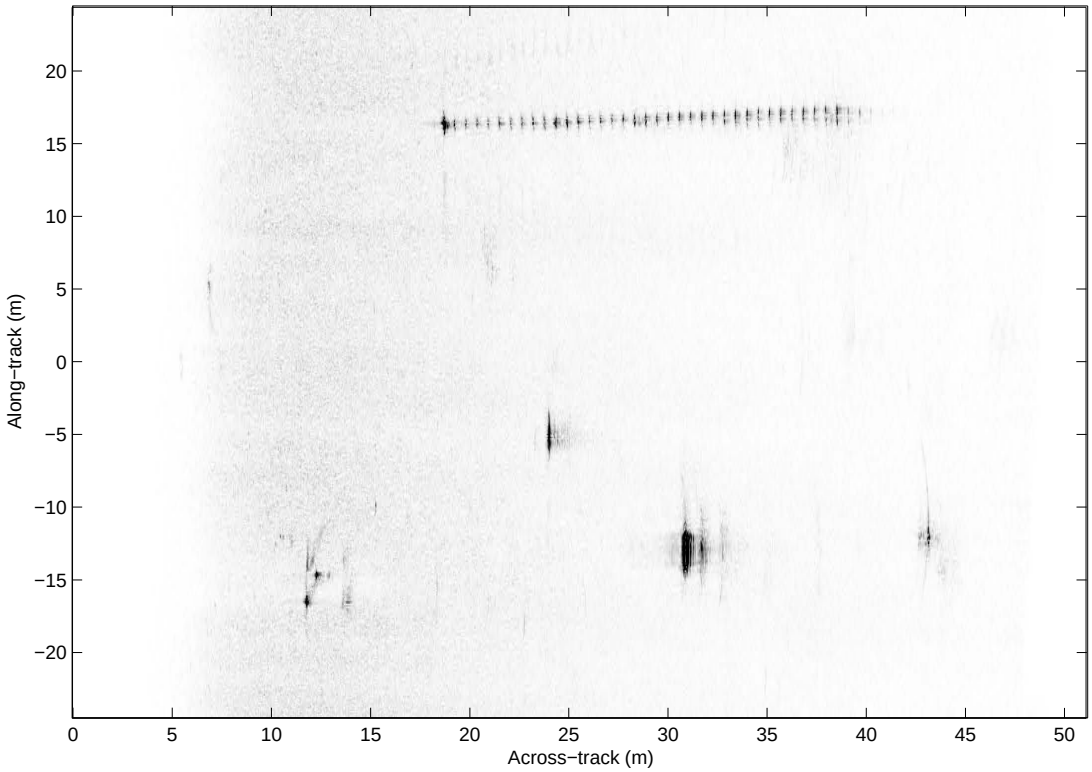

(b)

Fig. 4. Sydney Harbour data (a) reconstructed image without autofocus (b) SPGA autofocused image.

so are able to be used directly.

Non Lambertian scatterers — SPGA assumes that the energy scattered from a target is the same from all incidence angles. Because SPGA relies on beam symmetry for the linear slope estimation, targets that have non Lambertian scattering profiles can cause poor results.

Squinted systems — SPGA will not operate on systems that image with a squinted geometry (see above). However, if the squint angle is known, this can be compensated.

Bulk sway estimation — Approximations made in SPGA's derivation require that the sway is small—due to the wavenumber transform assuming no shift in the stationary phase point. SPGA should not be used for bulk sway estimation.

Platform yaw — A reliance on the spatial Doppler centroid makes the algorithm vulnerable to platform yaws. A yaw will shift the spatial Doppler centroid leading to poor linear slope estimation. SPGA assumes that no yaw is present in the system. This is the most severe restriction on SPGA.

VII. Conclusions and future work

The stripmap PGA extensions demonstrated in this paper operate well on simulated and field-collected data. The performance on a simulated scene consisting solely of point-like targets is limited only by the constraints of PGA's target windowing. From this we conclude that the SPGA method (and similarly, modified PCA) accurately models the wide-beam, wide-band nature of SAS imagery and is a successful extension of phase gradient techniques to stripmap geometries.

SPGA's use of local phase gradient estimation enhances its performance with respect to the modified PCA algorithm in situations where towfish yaw can be neglected. Even in the field-collected data with unknown yaw errors SPGA offers autofocus improvement (modified PCA diverged at the first iteration). Many of the limitations noted in the discussion are common to PGA based methods and some are shared by all sharpness-based algorithms. Unknown towfish yaw remains the primary limitation of the SPGA method (PCA is instead limited by the double integration of phase curvatures).

SPGA improvements include the use of a higher order eigenvector estimator [16] or the a better estimator of the local linear phase gradient. The local phase unwrapping method used by Ye *et. al* [17] has the potential to lift the restrictions imposed by platform yaw and may remove the need for local linear phase gradient estimation.

Acknowledgments

We would like to acknowledge partial sponsorship of the work by the Department of the Navy, NAVSEA Coastal Systems Staion, Panama City, Florida, USA as grant N61331-00-G003 and grant N61331-02-C-0031.

References

[1] W. G. Carrera, R. S. Goodman, and R. M. Majewski, *Spotlight synthetic aperture radar: signal processing algorithms*. Artech House, 1995.

[2] H. J. Callow, "Signal processing for synthetic aperture sonar image enhancement," PhD. thesis (under examination), April 2003.

[3] C. V. Jakowatz, Jnr., D. E. Wahl, P. H. Eichel, D. C. Ghiglia, and P. A. Thompson, *Spotlight-Mode Synthetic Aperture Radar: A Signal Processing Approach*. Boston: Kluwer Academic Publishers, 1996.

[4] D. E. Wahl, P. H. Eichel, D. C. Ghiglia, and C. V. Jakowatz, Jnr., "Phase gradient autofocus – a robust tool for high resolution SAR phase correction," *IEEE Transactions on Aerospace and Electronic Systems*, vol. 30, no. 3, pp. 827–835, July 1994.

[5] W. W. Bonifant, Jnr., "Interferometric synthetic aperture sonar processing," Master's thesis, Georgia Institute of Technology, July 1999.

[6] D. E. Wahl, C. V. Jakowatz, Jnr., and P. A. Thompson, "New approach to strip-map SAR autofocus," in *Sixth IEEE Digital Signal Processing Workshop*. IEEE, Oct. 1994, pp. 53–56.

[7] P. T. Gough and D. W. Hawkins, "Imaging algorithms for a strip-map synthetic aperture sonar: Minimizing the effects of aperture errors and aperture undersampling," *IEEE Journal of Oceanic Engineering*, vol. 22, no. 1, pp. 27–39, Jan. 1997.

[8] M. Soumekh, *Synthetic Aperture Radar Signal Processing with MATLAB Algorithms*. John Wiley & Sons, Inc., 1999.

[9] D. W. Hawkins, "Synthetic aperture imaging algorithms: with application to wide bandwidth sonar." Ph.D. dissertation, Department of Electrical and Electronic Engineering, University of Canterbury, Oct. 1996.

[10] P. T. Gough, M. P. Hayes, and H. J. Callow, "Strip-map path correction using phase matching autofocus," in *Proceedings of the fifth European Conference on Underwater Acoustics (ECUA) 2000*. ECUA, July 2000, pp. 412–418.

[11] M. P. Hayes, P. J. Barclay, P. T. Gough, and H. J. Callow, "Test results of a bathymetric synthetic aperture sonar," in *OCEANS 2001*, vol. 3. IEEE, November 2001, pp. 1682–1687.

[12] D. W. Warner, D. C. Ghiglia, A. FitzGerrell, and J. Beaver, "Two-dimensional phase gradient autofocus," *SPIE-Image Reconstruction from Incomplete Data*, vol. 4123, pp. 162–173, 2000.

[13] K. T. Knox and B. J. Thompson, "Recovery of images from atmospherically degraded short-exposure photographs," *Astrophysical Journal*, vol. 193, pp. L45–L48, Oct. 1974.

[14] J. D. Freeman, J. C. Christou, F. Roddier, D. W. McCarthy, Jnr., and M. L. Cobb, "Application of bispectrum analysis for phase recovery from one-dimensional infrared speckle data," *Journal of the Optical Society of America A*, vol. 5, no. 3, pp. 406–415, Mar. 1988.

[15] H. C. Chan and T. S. Yeo, "Noniterative quality phase-gradient autofocus (QPGA) algorithm for spotlight SAR imagery," *IEEE Transactions on Geoscience and Remote Sensing*, vol. 36, no. 5, pp. 1531–1539, Sept. 1998.

[16] C. V. Jakowatz, Jnr. and D. E. Wahl, "Eigenvector method for maximum-likelihood estimation of phase errors in synthetic-aperture-radar imagery," *Journal of the Optical Society of America*, vol. 10, no. 12, pp. 2539–2546, Dec. 1993.

[17] W. Ye, T. S. Yeo, and Z. Bao, "Weighted least-squares estimation of phase errors for SAR/ISAR autofocus," *IEEE Transactions on Geoscience and Remote Sensing*, vol. 37, no. 5, pp. 2487–2494, Sept. 1999.